ATLANTIS PRESS

Advances in Intelligent Systems Research, volume 165

International Conference on Modeling, Simulation, Optimization and Numerical Techniques (SMONT 2019)

Total Variation Minimization Enhanced Quantitative Microwave Induced Thermoacoustic Tomography using a GPU-accelerated Finite Element Method

Yunchao Jiang [1], Zhu Zheng [1], Min Wang [1] and Lei Yao [1,2,*]

[1]School of Electronic Science and Engineering (National Exemplary School of Microelectronics), University of Electronic Science and Technology of China, Chengdu, Sichuan, China

[2]Center for Information in Medicine, University of Electronic Science and Technology of China, Sichuan, China

[*]Corresponding author

***Abstract*—Microwave induced thermoacoustic tomography (MI-TAT) combines the advantages of microwave imaging and ultrasound imaging to obtain high-resolution and high-contrast biological tissue microwave energy absorption images. However, the current MI-TAT technique often gets images with a large number of artifacts or error results in the case of small number of sensors and limited detection angle. In this paper, we first introduction the total variation minimization (TVM) in the field of finite element method (FEM) based MI-TAT reconstruction algorithm and we can get perfect thermoacoustic image reconstruction with a small number of detectors and limited-angles. Since this approach is extremely computationally demanding, we apply the parallel strategy using a multi-core graphic-processing-unit (GPU) card to accelerate the calculation. The improved algorithm is verified and evaluated through simulations and phantom experiments, and the results suggest that our new method holds great potential in various clinical studies in the future.**

Keywords—thermoacoustic tomography; total variation minimization; finite element method; GPU acceleration

I. INTRODUCTION

Microwave induced thermoacoustic tomography (MI-TAT) as a hybrid imaging method has been widely studied these years. MI-TAT has excellent ultrasonic resolution and high electromagnetic contrast compared to conventional imaging methods. It has attracted considerable attentions, and a series of great progress has been made in diverse areas including breast cancer detection and diagnosis, brain imaging, and blood vasculature imaging [1-3]. Among various reconstruction approaches in MI-TAT, the finite element method (FEM) based quantitative MI-TAT reconstruction algorithm [4-5] might be particularly powerful and potentially valuable in practice. However, with the rising of noises in collected data, the quality of reconstructed images was getting worse, and the accuracy of the recovered values was affected considerably. In addition, in certain circumstance of MI-TAT applications, such as the breast cancer detection or the subcutaneous angiography, due to the specificity of physiological tissue and the consideration of reducing the cost in hardware or scanning time and signals could only be collected from a few numbers of transducers or capture signals in limited angle. It is very challenging for current quantitative MI-TAT reconstruction algorithm to obtain acceptable thermoacoustic images and accurate recovered values in cases the collected data is from few-detectors or limited-view.

Total variation minimization (TVM) is a powerful technique to reduce the noise sensitivity in image processing [6], thus in MI-TAT, developing a TVM enhanced reconstruction algorithm appears to be a good choice for us to overcome the limitations mentioned earlier. However, a primary challenge is that TVM enhanced iterative algorithms based on FEM are extremely computational demanding, since they require much more iterations to obtain converged results compared to their regular counterparts. It takes hours or even days to run the reconstruction algorithm to get a set of images with a typical mesh size for in vivo biological tissue imaging. Hence the use of the GPU based parallel strategy is required to promote calculative efficiency substantially.

In this study, we developed for the first time a TVM enhanced quantitative MI-TAT reconstruction algorithm and evaluate its capability to derive the absolute electrical conductivity with noisy data from fewer-detectors or limited-view. Then We use GPU-based multicore parallelism method to improve the computational efficiency of the algorithm. Phantom-like experiments were set to test the accuracy and efficiency of this improved method. The results show that our method is able to quantify the thermoacoustic properties in biological tissues accurately and efficiently.

II. METHODS

A. TVM Enhanced Quantitative MI-TAT Algorithm

In MI-TAT, a low frequency microwave is generally used as the excitation source to irradiate the sample, like a biological tissue. After absorbing the microwave energy, temperature of the biological tissue rises, which leads to thermal expansion and generates ultrasound waves. These waves, also called thermoacoustic (TA) waves, can be collected by ultrasonic transducers located on the boundary of the tissue, and then processed using different reconstruction algorithms to obtain maps of electromagnetic properties. The existing quantitative MI-TAT reconstruction algorithm consists of two steps.

The first one is to iterate compute the finite element solution of the time-domain thermoacoustic transmission equation [7] to get the loss density $s(\boldsymbol{r})$:

$$\nabla^2 p(\boldsymbol{r},t) - \frac{1}{c^2}\frac{\partial^2}{\partial t^2}p(\boldsymbol{r},t) = -\frac{\beta_e}{C_P}s(\boldsymbol{r})\cdot 2J(t)\frac{\partial J(t)}{\partial t} \quad (1)$$

Here $p(\boldsymbol{r},t)$ represent the acoustic pressure at time t and in position $\boldsymbol{r}$, here c is the acoustic speed, C_P represent the specific heat and β_e is the volume expansion coefficient, $s(\boldsymbol{r}) = \sigma \cdot |E_z(\boldsymbol{r})|^2$ is the power loss density, σ is the electrical conductivity, $E_z(\boldsymbol{r})$ denotes the spatial dependence of electric field and $J(t)$ denotes the microwave pulse function which is assumed as $J(t) = \delta(t - t_0)$ in these functions. In order to get an image from an initial guess of the power loss density distribution, we have to use another method to updating $s(\boldsymbol{r})$ from its initial value. We can use lease-squares minimization to update the computation results.

$$F(p,s) = \sum_{j=1}^{M}\left(p_j^o - p_j^c\right)^2 \quad (2)$$

Here, p_j^o represent the computed acoustic field data for $i = 1,2,\cdots M$ boundary locations. Meanwhile we can observe the boundary signals p_j^c in these boundary locations. We can get the equations by using the Newton method and updating $s(\boldsymbol{r})$ by iterative computation:

$$(\mathbf{J}^{\mathrm{T}}\mathbf{J} + \lambda\mathbf{I})\Delta\boldsymbol{\chi} = \mathbf{J}^{\mathrm{T}}(\mathbf{p}^{\mathrm{o}} - \mathbf{p}^{\mathrm{c}}) \quad (3)$$

Where $\mathbf{p}^o = (p_1^o, p_2^o, \cdots p_M^o)^T$ and $\mathbf{p}^c = (p_1^c, p_2^c, \cdots p_M^c)^T$; $\Delta\boldsymbol{\chi}$ represent the loss intensity updating vector; here, we use the Jacobi matrix to represent the $\frac{\partial p}{\partial s}$ results at the measurement sites; the Marquardt and Tikhonov regularization schemes parameters can be written as λ; and we use I to represent the identity matrix.

We can obtain the power loss density $s(\boldsymbol{r})$ from first step through the FEM iterator reconstruction algorithm; In second step, we should obtain the electrical conductivity $\sigma(\boldsymbol{r})$ from step one. We can use scalar Helmholtz equation for electromagnetic waves [3] to get $\sigma(\boldsymbol{r})$:

$$\nabla\cdot\left(\frac{1}{\mu_r}\nabla E_z\right) + k^2\varepsilon_r E_z = 0 \quad (4)$$

Here we use μ_r to represent the relative permeability, k is wave number, the equivalent relative permittivity constant can be written as ε_r which can be calculated as $\varepsilon_r = \varepsilon'_r + \frac{\sigma}{j\omega}$. the relative permittivity constant can be written as ε'_r and ω represent the microwave angular frequency.

We now incorporate the TVM framework within the first step of the algorithm. The total variation of the power loss density is applied by defining a new object function [6]:

$$\tilde{F}(p,s) = F(p,s) + L(s) \quad (5)$$

Here $L(s) = \int\sqrt{\omega_s^2|\nabla s|^2 + \delta^2}dxdy$ is the penalty term, we set two positive parameters ω_s and δ in this format and these two parameters can be determined numerically before run the algorithm. We can obtain the minimization of Equation (5) by differential calculation of $\tilde{F}$. Here $\tilde{F}$ represent each nodal parameter of $s(\boldsymbol{r})$ and the function can be written as:

$$\frac{\partial\tilde{\mathrm{F}}}{\partial \mathrm{s_i}} = -\sum_{\mathrm{j=1}}^{\mathrm{M}}\left(\mathrm{p_j^o} - \mathrm{p_j^c}\right)\frac{\partial \mathrm{p_j^c}}{\partial \mathrm{s_i}} + \mathrm{V_i} = 0,\ (\mathrm{i} = 1,2,\cdots \mathrm{N}) \quad (6)$$

Where $V_i = \frac{\partial L}{\partial s_i}$. Therefore, for TVM-based inversion, Equation (3) is modified as the following matrix equation:

$$(\mathbf{J}^T\mathbf{J} + \mathbf{R} + \lambda\mathbf{I})\Delta\boldsymbol{\chi} = \mathbf{J}^T(\mathbf{p}^o - \boldsymbol{p}^c) - \mathbf{V} \quad (7)$$

Where V is consisted of $\frac{\partial \mathbf{L}}{\partial s}$ and R is filled by $\frac{\partial \mathbf{V}}{\partial s}$.

B. Implementation of GPU-accelerated Code

Our parallel accelerate algorithm is based on NVIDIA's GPU and the developing toolkit is named "compute unified device architecture" (CUDA), The GPU framework offer us a cheap, powerful and easy operate tools to develop parallel algorithm. the flow diagram showed in Figure 1 of the FEM based quantitative MI-TAT reconstruction algorithm with TVM enhancement. Here the quantification of the electrical conductivity referring "step 2" of the algorithm is processed in CPU, for its calculation time is negligible compared to that of "step 1". In the reconstruction of power loss density $s(\boldsymbol{r})$, considering of each element in FEM solution is locality and sparsity, we realize the parallel calculation to achieve high computational speed with NVIDIA's CUDA framework. The GPU-accelerated code is developed and evaluated using the CUDA C/C++ programming platform based on cuBLAS, cuSPARSE, cuSOLVERS linear algebra libraries, and single precision data type for all variables and parameters were applied in the code to reduce computer storage requirements. The data transfer between the CPU ("host" in Figure 1) and the GPU ("device" in Figure 1) via PCI-e bus. In order to reduce the delay in data transmission, we design the algorithm to reduce data communication as much as possible. To further increase data transmission bandwidth and reduce data access time, we use CUDA share memory to obtain this goal. Finally, we transform the algorithm into a pipeline mode by using Hyper Q method and it significantly improve the operating rate.

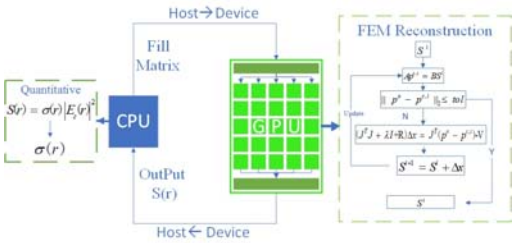

FIGURE I. THE FLOW DIAGRAM OF THE TVM ENHANCED QUANTITATIVE MI-TAT RECONSTRUCTION ALGORITHM

The above scheme as a basic optimization method significantly reduces the time the algorithm runs. The following two methods further improve the efficiency of the algorithm:1) assembling a new vector by the multiplication operation between a matrix and a vector; 2) solving linear matrix equation. In this work, matrices and vectors are divided and stored into different kernels named as "blocks" and "threads" and then the multiplication operations were applied simultaneously before the results were combined together, thus the calculation time can be reduced dramatically for the first procedure. When solving the thermoacoustic transmission equation $\mathbf{A}p^{c,i} = \mathbf{B}s^i$, we first calculate the inversion matrix of the global system matrix A and then obtained the thermoacoustic pressure $p^{c,i}$ by $p^{c,i} = \mathbf{A}^{-1}\mathbf{B}s^i$. Here a new approach is developed to achieve the inversion of the global system matrix A, which contains two steps: the Cholesky decomposition of the global system matrix $\mathbf{A} = \mathbf{L}\mathbf{L}^T$, where L is a low triangular matrix, and we use iterative conjugate gradient solver to solve the matrix equation $\mathbf{L}\mathbf{L}^T\mathbf{A}^{-1} = \mathbf{I}$, hence the calculative efficiency in the second procedure can be raised greatly.

In the inverse model, the most time-consuming procedure in the GPU-accelerated code is the computation of the Jacobian matrix **J** in equation (7). Instead of using several kernels to calculate each individual columns of the Jacobian matrix sequentially, we successfully assembled the whole Jacobian matrix **J** in one time by making the use of the developed new approach to achieve the inversion of the global system matrix A. We furthermore improve the parallel degree of other parts in the inverse model using similar ways in the forward model and increase the computational efficiency dramatically.

We use various of experimental data to validate our GPU-accelerated algorithm. The reconstructed images of electrical conductivity were compared to those using the existing unparalleled CPU-based algorithm, in all the experimental cases the relative errors between these two methods were less than 1%, though different precision data type for all variables and parameters were applied in these codes.

III. RESULTS

We demonstrate the ability of our TVM enhanced MI-TAT reconstruction algorithm through several tissue-like phantom experiments. Figure 2 depicts the schematic of the MI-TAT system we used in these experiments. In our experimental system, we use a 3.0 GHz pulsed microwave source to generate pulse signals. The bandwidth of signals is 50MHZ and the pulse duration is 700ns. The time we obtain pulse signals, we use a 10dB gain horn antenna to radiate the microwave signals. We place the phantom below the antenna and in order to decrease the microwave/ultrasound signal transmission attenuation, the phantom is immersed by oil in a tank. We use unfocused transduce to gain microwave/ultrasound signals. The center frequency of transducer is 2.25MHZ. we mount the transducer on a step moto to rotate around the phantom. The step moto is made by Beijing Zolix Instruments Co., Ltd, Beijing, China. The distance between transducer and phantom is 70mm and rotate around the phantom by the step moto. After the signals obtain from the transducer, the computer converts analog signals to digital signals and postprocess soon. We use LabView programming to control the equipment and make some preprocess of signals.

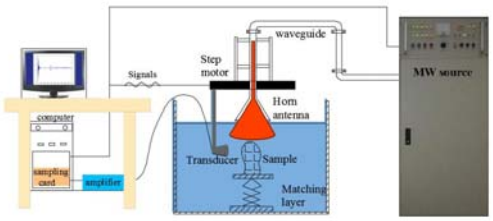

FIGURE II. THE SCHEMATIC OF MI-TAT SYSTEM

Three experimental cases were conducted in this work. In each case, a single cylindrical salty phantom with various size and electromagnetic properties was immersed in ion water and used as a sample to generate thermoacoustic wave when induced by the microwave. In the first experiment, the diameter of the phantom was 3 mm and the salt concentration 3% which made its electrical conductivity as $4.85\ s/m$. The ultrasound transducer was rotated along the surface of the 104mm-diameter circular background over 360° region with a step size of 8°, indicate that 45 measurements in total were collected during the scanning procedure. In the second experiment, the diameter of the phantom was 5 mm and the salt concentration 2% which we could figure out its electrical conductivity was $3.42\ s/m$. The ultrasound transducer was rotated along the background surface over 360° degree with a step size of 12°, which means that only 30 measurements were collected during the scanning procedure. In the last experiment, the diameter of the phantom was 3 mm and the salt concentration of the phantom was 5% which represents its electrical conductivity was $6.95\ s/m$. The transducer was rotated along the surface of the background within only 90° view (a region close to the target) with a step size of 3°, which added up to 30 measurements were collected during the scanning procedure. The relative permittivity in all cases was 59.0 , 63.0 and 55.0, respectfully.

The experimental data of these phantoms was reconstructed using dual mesh pair based on our GPU-accelerated TVM enhanced MI-TAT reconstruction algorithm. For comparison purpose, results from regular MI-TAT reconstruction algorithm were also presented. The regular method obtain result images after three iterator calculate and the TVM-enhanced method get results by fifteen iterators. The parameters $\omega_s = 1.0 \times 10^{-3}$ and $\delta = 1.0 \times 10^{-4}$ were used based on numerical tests in this study.

Figure 3 displays the reconstructed electrical conductivity images and the quantitative conductivity value line through the center of the targets. We find that, though measurements were insufficient (case 1 and 2), or data was collected within limited view (case 3), the targets could still be clearly recovered with accurate size, position, and electrical conductivity using TVM enhanced MI-TAT algorithm (Figs. 3d-f), while on the other hand, strong artifacts always appear in images from regular MI-TAT method (Figs. 3a-c). These artifacts generally are shown far from the detector positions where the measurement sensitivity is highest, however, such severe artifacts are damped remarkably based on the TVM enhancement.

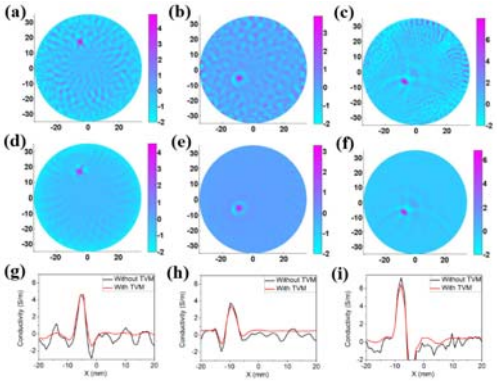

FIGURE III. TRECONSTRUCTED RESULTS FOR THE THREE PHANTOM EXPERIMENTAL CASES. (A-C) RECONSTRUCTED ELECTRICAL CONDUCTIVITY IMAGES BASED ON REGULAR METHOD, (D-F) RECONSTRUCTED ELECTRICAL CONDUCTIVITY IMAGES BASED ON TVM ENHANCED METHOD, (G-I) QUANTITATIVE CONDUCTIVITY VALUE CURVE THROUGH THE CENTERS OF THE TARGETS

Table 1 provides the quantitative comparison among the actual and reconstructed value from the methods with and without TVM enhancement. The recovered target size was estimated based on the full-width-half-maximum (FWHM) of the object. Meanwhile the recovered electrical conductivity of the target was determined from a region-of-interest (ROI) based on the center and the FWHM of each object. We see that the values of recovered target size from both methods are very close to the actual ones, while the electrical conductivity values of the target are well recovered quantitatively based on the TVM enhanced method as seen from Table 1.

TABLE I. COMPARISON OF RECOVERED VALUES BETWEEN THE REGULAR METHOD AND TVM ENHANCED METHOD

Phantom case #	**Target size (*mm*)**			**Conductivity of the target (s/m)**		
	Exact	***Regular method***	***TVM enhanced method***	***Exact***	***Regular method***	***TVM enhanced method***
1	3	2.6	2.6	4.85	4.96	4.81
2	5	4.25	4.3	3.42	3.90	3.60
3	3	2.6	2.6	6.95	7.90	6.70

We then validate the acceleration of GPU-accelerated code on different size of meshes and compared the results of the reconstruct results based on the CPU. We list the computation time and speed-up ratio base on the GPU-accelerate code and CPU code with different mesh size on Table 2. The CPU is Intel i7-6700, and the GPU is NVIDIA GeForce GTX Titan X. We can see clearly from Table 2 that the GPU-enhanced algorithm has a huge improvement in computation time compared to the CPU-based computing. Taking account of the fact that in order to obtain stable and converged reconstruction results TVM enhanced algorithm always requires much more iterations than regular method does (for example, fifteen against three in this study), this improvement is vital and necessary when applying TVM enhanced MI-TAT reconstruction algorithm in practice. It is also note that the acceleration ratio increased with increasing mesh size, indicating that the GPU-based parallel algorithm has a great advantage of dealing with larger mesh. However, we find that when the mesh size reaches a certain density, for example, 5,977 nodes in fine mesh and 1,525 nodes in coarse mesh in this case [8], the improvement of the acceleration ratio is kind of limited. One possible reason is that the efficiency of achieving the inversion of the global system matrix A in the GPU-based parallel code becomes lower with larger volume data exchange. We also note that all the relative errors are less than 1%, which demonstrates that the single precision GPU accelerate algorithm can also provide effective accuracy results.

TABLE II. PERFORMANCE COMPARISON BETWEEN GPU AND CPU UNDER DIFFERENT COMPUTING SCENARIOS

Dual Mesh Pair	**GPU (sec)**	**CPU (sec)**	**Acceleration Ratio**
630-2457	2.13	370.11	173.8
930-3,627	4.70	1,504.00	320.0
1,525-5,977	13.50	7,695.63	570.0
3,542-13,973	135.80	80,006.50	589.1

IV. CONCLUSION

In summary, we have proposed a TVM enhanced quantitative MI-TAT reconstruction algorithm that obtain a brilliant conductivity results from heterogeneous turbid media. We design numerical simulation and phantom experiments to compare GPU parallel algorithm and conventional CPU serial algorithm one by one. the comparative study clearly shows that the strategy of incorporating TVM into MI-TAT reconstruction algorithm results in significant optimization in image quality and notable accuracy in quantifying electrical conductivity, especially in cases noisy data are collected from fewer-detectors or limited-view. In addition, we have implemented the GPU based parallel code to accelerate the calculation in TVM enhanced MI-TAT algorithm, and successfully demonstrated its performance. Our results show that the speed up ratio between the reconstructions from GPU-accelerate code and the CPU-based code could exceed a factor of 500 times while providing sufficient accuracy. The work presented here suggests that our TVM enhanced MI-TAT method based on the GPU acceleration can be a promising powerful and inexpensive biomedical imaging tool for clinical studies in the future.

ACKNOWLEDGMENT

This study is supported by National Natural Science Foundation of China (11674047).

REFERENCES

[1] R. Kruger, D. Reinecke, and G. Kruger, “Thermoacoustic computed tomography–technical considerations”, Med. Phys. 26,1999, 1832-1837.

[2] M. Pramanik, G. Ku, C. Li, and L. V. Wang, “Design and evaluation of a novel breast cancer detection system combining both thermoacoustic (TA) and photoacoustic (PA) tomography”, Med. Phys,35,2008, 2218-2223.

[3] W. Ding, Z. Ji, D. Xing. “Microwave-excited ultrasound and thermoacoustic dual imaging”, Appl. Phys. Lett, 110,2017, 183701.

[4] L Yao, G Guo, H Jiang, “Quantitative microwave induced thermoacoustic tomography”, Med. Phys,37,2010,3752-3759.

[5] L. Huang, L. Yao, L. Liu, et.al, “Quantitative thermoacoustic tomography: Recovery of conductivity maps of heterogeneous media”, Appl. Phys. Lett,101,2012,2010–2013.

[6] D. Dobson, F. Santosa, “An image-enhancement technique for electrical impedance tomography”, Inverse Probl,10,1994,317–334.

[7] A. Mashal, J. H. Booske, S. C. Hagness, “Toward contrast-enhanced microwave-induced thermoacoustic imaging of breast cancer: An experimentalstudy of the effects of microbubbles on simple thermoacoustic targets”, Phys. Med. Biol. 54,2009,641–650.

[8] X.Gu, Y.Xu, H.Jiang, “Mesh-based enhancement schemes in diffuse optical tomography”, Med. Phys,30,2003,861-869.